Energy dependence of the exchange-correlation kernel of time-dependent density functional theory: A simple model for solids

Silvana Botti, Armel Fourreau, François Nguyen, Yves-Olivier Renault, Francesco Sottile, and Lucia Reining
Laboratoire des Solides Irradiés, UMR 7642 CNRS/CEA, Ecole Polytechnique, 91128 Palaiseau, France
(Received 25 March 2005; revised manuscript received 23 June 2005; published 6 September 2005)

Time-dependent density functional theory faces an important problem when it comes to extended systems: The long-range component of the exchange-correlation kernel f_{xc} is completely absent from local density or generalized gradient approximations, but it is believed to be present in the "exact" f_{xc}. Several attempts have been made to solve this issue, the simplest of them being the use of a model static long-range kernel of the form $-\alpha^{static}/q^2$. In this paper, we propose and motivate a dynamical extension of this model of the form $-(\alpha+\beta\omega^2)/q^2$. The dynamical model is then used to calculate the dielectric function of a large variety of semiconductors and insulators. The absorption spectra of large gap insulators are remarkably improved with respect to calculations where the kernel is taken to be static. This approach is valid also for energies in the range of plasmons, and hence it yields, e.g., good electron energy loss spectra. Finally, we present some simple theoretical arguments that relate the parameters of the model to physical quantities, like the dielectric constant and the plasmon frequency.

DOI: 10.1103/PhysRevB.72.125203 PACS number(s): 71.10.−w, 78.20.Bh, 71.35.−y, 71.15.Qe

I. INTRODUCTION

In order to understand the electronic properties of materials, especially in the context of transport and optical excitations, it is essential to have a solid knowledge of the electron-electron and electron-hole interaction. The electronic structure of semiconductors and insulators is nowadays well described by reliable *ab initio* methods.[1–3] Optical properties can then be calculated starting from these electronic structures. The simplest approach consists in looking at spectra obtained as a sum of independent transitions between Kohn-Sham (KS) or quasiparticle states. Unfortunately, this method is known to exhibit severe shortcomings compared to experiments.[4] The next step is the so-called random phase approximation (RPA), that includes the effects due to the variation of the Hartree potential upon excitation. However, this approximation does not lead to any significant improvement for most solids, especially if there are no particularly pronounced polarizable inhomogeneities in the charge density. It is the neglect of variations of the exchange-correlation (xc) potential, which include the effect of the electron-hole Coulomb interaction, that is responsible for an overall disagreement in the absorption strength (typically the absorption strength is underestimated at low energies and overestimated at high energies), as well as for the complete failure when it comes to reproduce bound excitons. Early attempts to overcome the problem by including two-quasiparticle effects were accomplished successfully using the effective-mass approximation[5] for bound excitons, and the solution of the Bethe-Salpeter equation (BSE) in a tight-binding approximation[6] for continuum spectra. Later, the BSE was solved on the basis of more realistic band structures.[7–11] In these works, the BSE was essentially written as an effective two-particle Schrödinger equation that contained the electron-hole interaction. The agreement with experiment was greatly improved with respect to calculations within the RPA, but of course, the associated computational cost became relatively large.

The problem of the calculation of neutral (e.g., optical) excitations can be viewed from a different perspective by using the generalization of static density functional theory (DFT) to time-dependent problems.[12,13] In time-dependent DFT (TDDFT) all observables, as well as the time-dependent wave functions and potentials, are functionals of the time-dependent density. In the linear response regime, TDDFT reduces to the solution of a two-point Dyson-type equation for the response function, that can be treated in a computationally efficient way. One could therefore hope to replace the more cumbersome four-point BSE method. The basic ingredient entering the response equation, besides the KS independent particle response function $\chi^{(0)}$ and the variation of the Hartree potential already present in the RPA, is the so-called exchange-correlation kernel f_{xc}. This quantity is defined as the functional derivative of the xc potential with respect to the density $f_{xc}(\mathbf{r},\mathbf{r}',t,t')=\delta v_{xc}(\mathbf{r},t)/\delta\rho(\mathbf{r}',t')$. Its functional form is unknown, and appears to be quite difficult to model. Nevertheless, this term is essential as its task is to modify the excitation energies and to redistribute the oscillator strength. Note that the RPA can be recovered by setting $f_{xc}=0$.

It turns out that TDDFT can yield good results using the local density approximation (LDA) for the xc potential and the adiabatic local density approximation (TDLDA)[14] for the xc kernel,

$$f_{xc}^{TDLDA}(\mathbf{r},\mathbf{r}',t,t') = \delta(\mathbf{r}-\mathbf{r}')\frac{dv_{xc}^{LDA}[\rho(\mathbf{r})]}{d\rho(\mathbf{r})}\delta(t-t'). \quad (1)$$

This is true especially when finite systems are concerned, but also electron energy loss spectra (EELS) of solids at low momentum transfer are often well described within the TDLDA.[7,15] However, in both cases already a large improvement with respect to the independent-particle KS spectrum (i.e., with respect to a simple sum over independent transitions between KS states) comes from the density variation of

the Hartree potential. This term is of course included in the TDLDA in the same way as in the RPA. On the other hand, in the case of solids the Hartree contribution is not sufficient to yield good absorption spectra (it then just gives rise to the crystal local field effects). In this case, taking into account f_{xc} within TDLDA does not lead to a significant (if at all) improvement.[16] The reason for this failure can be traced back to the short-range nature of the TDLDA f_{xc}, while the "exact" f_{xc} is believed to be long ranged,[7,17] decaying in momentum space as $1/q^2$.

Therefore, when calculating electronic excitations in solids we face a dilemma. We have the BSE, a precise but computationally demanding method, and TDDFT, a rather inexpensive method but whose applicability is severely limited by the shortcomings of the TDLDA. As such, it would be extremely desirable to find a better, generally applicable f_{xc} to be used in conjunction with an electronic structure calculated from a suitable potential. Improvements to the TDLDA might come through the inclusion of dynamical (memory) effects and/or long-range nonlocal terms.[13,18] Indeed, a big effort has been made in this latter direction from quite different viewpoints, like time-dependent current density functional theory,[19] perturbative approaches,[18,20] or exact-exchange approximations to the kernel.[21–23] Several of the kernels proposed in the literature were also tested in the simplest extended system, i.e., the homogeneous electron gas.[24] Furthermore, in Ref. 19, the effective long-range kernel proposed to improve the TDLDA results was applied to bulk semiconductors, like silicon and diamond. In Ref. 23, the exact-exchange formalism illustrated in Ref. 22 is used to obtain the absorption spectrum of silicon and again, the result is considerably improved with respect to the RPA or TDLDA. Nevertheless, this approach is computationally cumbersome and the neglecting of correlation leads to a collapse of the spectrum. The inconvenience is solved by the introduction of an empirical cutoff of the Coulomb interaction, which simulates the missing screening.

A class of kernels that was shown to be very efficient in the description of solids consists of those directly derived from the BSE. A parameter-free expression was obtained in several different ways (by a first order expansion of the screened Coulomb interaction W, by mapping the matrix elements of the BSE on those of the TDDFT, or by introducing density variations into the Hedin's equations), leading to the same formula.[7,25–32] The results obtained using this kernel, in conjunction with a quasiparticle band structure, are in excellent agreement with those of the BSE. For a more exhaustive compendium, we invite the reader to refer to Ref. 7. Although involving a potentially reduced computational effort with respect to the BSE, these calculations are still significantly more cumbersome than those within the RPA or the TDLDA. Therefore, the question of finding reliable and efficient models for f_{xc} remains open. There are nevertheless several important results that we can learn from these kernels. In particular, it was shown that the *ab initio* expression of Ref. 25 has the asymptotic form of a long-range contribution (LRC)

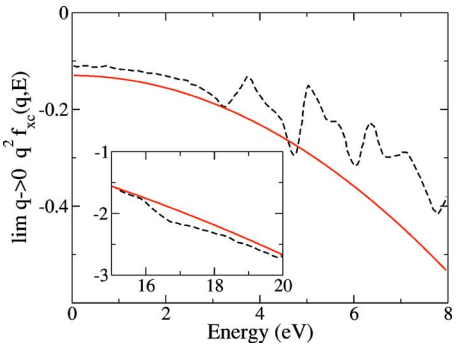

FIG. 1. (Color online) Real part of the LRC component of the xc kernel for silicon. The inset shows the same function in an energy region close to the plasma frequency. Dashed lines, calculation from Ref. 35; solid line, the present model.

$$f_{xc}^{static}(\mathbf{q}) = -\frac{\alpha^{static}}{q^2}, \tag{2}$$

where α^{static} is a material dependent parameter. Keeping only this contribution is sufficient to simulate the strong continuum exciton effect in the absorption spectrum and in the refraction index of several simple semiconductors, like bulk silicon or GaAs, provided that quasiparticle energies are used as a starting point. The parameter α^{static} was shown to be inversely proportional to the macroscopic dielectric constant.[30] This allows one to predict the absorption spectrum starting from the knowledge of the experimental dielectric constant of the material in question. However, the model f_{xc}^{static} of Eq. (2) has some weaknesses that become evident when the band-gap increases. For example, in diamond the first shoulder and the main peak in the spectrum cannot be described with good precision[30] using a frequency independent parameter α^{static}. The problem gets even more serious when bound exciton peaks appear in the spectrum, e.g., as for MgO (Ref. 30) and solid argon.[33] Finally, when the whole spectral range including plasmons is considered, the approximation completely breaks down. In fact, in order to describe the plasmon of, e.g., silicon, one could still use Eq. (2), but with an α^{static} that is an order of magnitude larger than the one that yields a good optical spectrum.[30]

Obviously, a widely valid but still simple model for f_{xc} would have a significant impact—in fact, already the limited, static LRC model, for example, has opened the way for the efficient calculation of optical properties of complex systems such as superlattices.[34] In order to improve on the model (2) we can follow basically two paths: (i) introduce a more complex spatial behavior; (ii) introduce a frequency dependence. In this paper we follow the latter path proposing a model kernel of the form

$$f_{xc}^{dyn}(\mathbf{q},\omega) = -\frac{1}{q^2}(\alpha + \beta\omega^2). \tag{3}$$

In this choice we were guided by recent calculations[35] for bulk silicon and diamond, that yielded the frequency dependence of the long-range term of the xc kernel from the inversion of the BSE (see the dashed lines in Fig. 1 and the original figures of Ref. 35). Thanks to a simple analytical

model, we prove that the two parameters α and β of Eq. (3) can be related to physical quantities, like the dielectric constant and the plasma frequency. These relations are validated by comparison with the values of α and β fitted to reproduce as close as possible the experimental spectra. Having α and β, we use $f_{\mathrm{xc}}^{\mathrm{dyn}}$ of Eq. (3) to calculate the absorption spectra of bulk silicon, gallium arsenide, aluminum arsenide, silicon carbide, diamond, cadmium selenide, lithium fluoride, and the EELS of silicon. The real and imaginary parts of the macroscopic dielectric functions ε_M and the loss spectrum are well reproduced when this frequency-dependent long-range component is taken into account. This is true to a certain extent even in the presence of bound excitons.

This paper is structured as follows. Section II motivates the model on the basis of the results of Ref. 26. Section III includes the applications to real materials mentioned above, as well as a discussion of the material dependence of the parameters of the model. Finally, we draw our conclusions in Sec. IV.

II. THE MODEL

In order to derive the model kernel (3) proposed here, we follow a slightly different path than the one used to derive its static version.[25] In fact, we can directly start from the explicitly frequency-dependent expression for the xc kernel that was given in Ref. 26,

$$f_{\mathrm{xc,res}}^{\mathbf{GG}'}(\mathbf{q},\omega) \sim \left[\chi_{\mathbf{GG}_1}^{(0)}(\mathbf{q},\omega)\right]^{-1} \sum_{\substack{v'c'\mathbf{k}' \\ vc\mathbf{k}}} \frac{\Phi_{\mathbf{G}_1}^{*}(vc\mathbf{k};\mathbf{q})}{\epsilon_{c\mathbf{k}}-\epsilon_{v\mathbf{k}}-\omega-i\eta} \times W_{\substack{vc\mathbf{k} \\ v'c'\mathbf{k}'}} \frac{\Phi_{\mathbf{G}_2}(v'c'\mathbf{k}';\mathbf{q})}{\epsilon_{c'\mathbf{k}'}-\epsilon_{v'\mathbf{k}'}-\omega-i\eta} \times \left[\chi_{\mathbf{G}_2\mathbf{G}'}^{(0)}(\mathbf{q},\omega)\right]^{-1}. \quad (4)$$

In Eq. (4) we write only the resonant (res) contribution, but we use of course also the corresponding antiresonant (antires) one [where $(\omega+i\eta)\rightarrow-(\omega+i\eta)$]. $\chi_{\mathbf{GG}}^{(0)}$ is the independent-particle response function using quasiparticle energies, $\mathbf{k}$ is a wave vector in the Brillouin zone, $\mathbf{G}$ is a reciprocal lattice vector, $\mathbf{q}$ is the wave vector of the perturbation, which is supposed to be vanishingly small at the end, $\{j\mathbf{k}\}$ indicates a KS state defined by the band index j and the $\mathbf{k}$ vector and $\epsilon_{j\mathbf{k}}$ the corresponding quasiparticle eigenvalue, Φ is the product of a valence v and conduction c KS orbital, and W is the matrix element of the statically screened Coulomb interaction between four KS orbitals, as explained in Ref. 26.

We limit the study of Eq. (4) only to the $\mathbf{G}=\mathbf{G}'=0$ elements of all matrices which, as we verified, is a good approximation for all the materials studied here.[36] To obtain the overall frequency dependence of the expression (4), we simplify the response function by applying the simple model of a single Lorentz oscillator[37] with resonance frequency ω_g to calculate the independent-particle response $\chi^{(0)}$,

$$\chi_{\mathbf{00}}^{(0)}(\mathbf{q},\omega) = -2\sum_{vc\mathbf{k}} \frac{\Phi_0^{*}(vc\mathbf{k};\mathbf{q})\Phi_0(vc\mathbf{k};\mathbf{q})}{\epsilon_{c\mathbf{k}}-\epsilon_{v\mathbf{k}}-\omega-i\eta} + \text{antires}. \quad (5)$$

If we insert in Eq. (5) the approximation $\Phi(vc\mathbf{k};0) \approx b\, q/(\epsilon_{c\mathbf{k}}-\epsilon_{v\mathbf{k}}) \approx b\, q/\omega_g$, where b is a material dependent constant, we obtain

$$\chi_{\mathbf{00}}^{(0)}(\mathbf{q},\omega) \sim -\frac{q^2|b|^2}{\omega_g}\frac{1}{\omega_g^2-\omega^2-2i\eta\omega}. \quad (6)$$

The constant b can be related to the plasma frequency ω_p by the f-sum rule[38] for the imaginary part of the macroscopic dielectric function ε_M:

$$\int_0^{\infty} d\omega\omega\, \mathrm{Im}\, \varepsilon_M(\omega) \sim \omega_p^2. \quad (7)$$

Remembering that within the RPA,

$$\varepsilon_M(\omega) = 1 - \lim_{q\rightarrow 0}\frac{4\pi}{q^2}\chi_{\mathbf{00}}^{(0)}(\mathbf{q},\omega), \quad (8)$$

we can use Eq. (7) together with the single oscillator model (6) to deduce

$$\int_0^{\infty} d\omega\omega\, \mathrm{Im}\, \varepsilon_M(\omega) \approx \int_0^{\infty} d\omega\omega \frac{|b|^2}{\omega_g^2}\delta(\omega-\omega_g) \sim \frac{|b|^2}{\omega_g} \sim \omega_p^2. \quad (9)$$

Setting together Eqs. (6) and (9) we recover the familiar Lorentz oscillator expression

$$\chi_{\mathbf{00}}^{(0)}(\mathbf{q},\omega) \sim -q^2\frac{\omega_p^2}{\omega_g^2-\omega^2-2i\omega\eta}, \quad (10)$$

where ω_g is the resonance frequency, which corresponds here to the mean transition energy in the range of strong absorption calculated within the RPA and using quasiparticle energies, and η gives the damping coefficient of the harmonic oscillator which determines the width of the resonance peak.

Inserting all the ingredients above to simplify Eq. (4) we can finally write

$$f_{\mathrm{xc,res}}^{\mathbf{00}}(\mathbf{q},\omega) \sim -\frac{1}{q^2}\frac{\bar{W}}{\omega_p^2\omega_g}\frac{(\omega_g^2-\omega^2-2i\eta\omega)^2}{(\omega_g-\omega-i\eta)^2}, \quad (11)$$

where $\bar{W}$ is an effective screened Coulomb interaction, which is proportional to the inverse dielectric constant $\varepsilon_M(0)$. The antiresonant contribution is treated in an analogous way, yielding

$$f_{\mathrm{xc,antires}}^{\mathbf{00}}(\mathbf{q},\omega) \sim -\frac{1}{q^2}\frac{\bar{W}}{\omega_p^2\omega_g}\frac{(\omega_g^2-\omega^2-2i\eta\omega)^2}{(\omega_g+\omega+i\eta)^2}. \quad (12)$$

Adding up the two terms (11) and (12) we arrive at the final result,

TABLE I. Steps leading to the determination of optical spectra using ABINIT (Ref. 43) and the DP code (Ref. 45).

	Description	Approximations involved
STEP 1:	A ground state DFT calculation, using as xc potential $V_{xc}=V_{xc}^{LDA}$, gives the electronic band structure in terms of the KS-LDA wave functions ϕ_i and eigenvalues ϵ_i.	Choice of V_{xc} and of the pseudopotentials.
STEP 2:	The independent-particle polarizability $\chi^{(0)}$ is built using wave functions and eigenvalues obtained in step 1.	None, except the linear response framework.
STEP 3:	KS-LDA eigenvalues are replaced by quasiparticle GW eigenvalues in the calculation of $\chi^{(0)}$. (Only for LRC calculations.)	GW approximation for quasiparticle energies and KS-LDA wave functions ϕ_i.
STEP 4:	The full polarizability χ is obtained from Eq. (17).	Choice of f_{xc}. In RPA $f_{xc}=0$. In TDDLA f_{xc} is given by Eq. (1). We also use for f_{xc} the static scalar model of Eq. (2) and the dynamical scalar model of Eq. (3).
STEP 5:	The dielectric function, calculated as $\varepsilon^{-1}=1+v\chi$ gives both absorption and EELS via the macroscopic dielectric function $\varepsilon_M=1/\varepsilon_{00}^{-1}$.	None.

$$f_{xc}^{dyn}(\mathbf{q},\omega) \sim -\frac{1}{q^2}\frac{\bar{W}}{\omega_p^2\omega_g}(\omega_g^2+\omega^2+i\eta\omega). \tag{13}$$

In the following we neglect the imaginary part of f_{xc}^{dyn}, as it looks reasonable to suppose that it is always significantly smaller than the real part. Equation (13) has the form of the dynamical model kernel of Eq. (3), provided that

$$\alpha \sim \frac{\omega_g}{\varepsilon_M(0)\omega_p^2}, \quad \beta \sim \frac{1}{\varepsilon_M(0)\omega_p^2\omega_g}. \tag{14}$$

In contrast to f_{xc}^{static}, f_{xc}^{dyn} includes a long-range term quadratic on the frequency. In order to use the dynamical LRC approach not only for understanding the role of f_{xc}, but also for predicting optical properties of semiconductors and insulators with a low computational effort, it is essential to be able to express the two parameters as functions of known physical quantities, as it was done for the parameter α^{static} in Ref. 30. More precisely, α^{static} was shown to be inversely proportional to the dielectric constant. Also here it turns out that both the static and the quadratic term are inversely proportional to the dielectric constant. Moreover, we find an additional dependence of our model parameters on the plasma frequency ω_p and the average absorption gap ω_g.

Finally, it is interesting to observe the correspondence between the short-range contact exciton model,[39–41] which is known to yield a good description of continuum exciton effects, and the LRC kernel approximation in TDDFT. In fact, the contact exciton equation

$$[\varepsilon_M(\omega)-1] = \frac{[\varepsilon_M^{RPA}(\omega)-1]}{1+g(\varepsilon_{M(\omega)}^{RPA}-1)} \tag{15}$$

is equivalent to the LRC kernel approximation in TDDFT,[33,35] provided that $f_{xc}=-g4\pi/q^2$. In Ref. 39 the parameter g is shown to be proportional to ω^2/b^2, similarly to the parameter β of our model. Nevertheless, we verified that such a model kernel with only the frequency dependent term would not be sufficient to yield good spectra on a large frequency range (e.g., to reproduce both absorption and EELS of silicon).

III. APPLICATIONS

A. Calculations

For our numerical calculations we follow the procedure summarized in Table I. We use the same computational parameters[42] as Ref. 30: the resulting spectra are well converged and can be directly compared to the ones obtained with the static kernel in Ref. 30. We first determined the ground state lattice constants, charge densities, and the DFT-LDA KS electronic structures (step 1 in Table I), using norm-conserving pseudopotentials and a plane wave basis.[43] All spectra are calculated at the theoretical lattice constants. We then constructed the independent-particle response function $\chi^{(0)}$ (step 2 in Table I). In case of calculations including either a static or a dynamical LRC kernel, we followed the suggestion of Ref. 25, i.e., we used KS DFT-LDA wave functions together with quasiparticle eigenvalues calculated in the GW approximation[44] (step 3 in Table I). In case of TDLDA calculations instead we used as usual KS DFT-LDA wave functions together with KS DFT-LDA eigenvalues. This can be understood remembering that the xc kernel can be decomposed in two terms

$$f_{xc}=f_{xc}^{(1)}+f_{xc}^{(2)}, \tag{16}$$

where $f_{xc}^{(1)}$ transforms the KS response function into the independent quasiparticle one and $f_{xc}^{(2)}$ accounts for the electron-hole interaction.[31,32] Like the full expression from which it is derived, our model kernel is meant to simulate

TABLE II. Experimental dielectric constants, plasma frequency calculated from the theoretical average electron density, and parameters α and β which gave the best fit for the absorption spectra calculated in this work. In the last column the resonance frequency evaluated by inserting the fitted α and β in Eq. (13). LiF is the only case where the value of ω_g is not in the middle of the range of absorption.

Crystal	$\varepsilon_M(0)$	ω_p (eV)	α	β ($\mathrm{eV}^{-2}\times 10^{-3}$)	ω_g (eV)
Si	11.4	17.05	0.13	6.35	4.5
GaAs	10.9	15.82	0.15	7.43	4.5
AlAs	8.2	15.77	0.20	10.54	4.4
SiC	6.5	23.29	0.20	4.05	7.0
CdSe	5.8	14.55	0.45	14.86	5.5
C	5.6	31.87	0.28	1.35	14.4
LiF	1.96	25.5	1.50	33.76	6.7

only the second part $f_{\mathrm{xc}}^{(2)}$ of the xc kernel, which is responsible for excitonic effects. Finally, we performed a TDDFT calculation in frequency and reciprocal space[45] by solving the matrix equation

$$\chi_{\mathbf{GG}'}(\mathbf{q},\omega)=\chi^{(0)}_{\mathbf{GG}'}(\mathbf{q},\omega)+\chi^{(0)}_{\mathbf{GG}_1}(\mathbf{q},\omega)\Big[v_{\mathbf{G}_1}(\mathbf{q})\delta_{\mathbf{G}_1\mathbf{G}_2}+f_{\mathrm{xc}}^{\mathbf{G}_1\mathbf{G}_2}(\mathbf{q},\omega)\delta_{\mathbf{G}_1\mathbf{0}}\delta_{\mathbf{G}_2\mathbf{0}}\Big]\chi_{\mathbf{G}_2\mathbf{G}'}(\mathbf{q},\omega), \quad (17)$$

where v is the bare Coulomb interaction (step 4 in Table I). The matrix $\chi_{\mathbf{G},\mathbf{G}'}$ is the linear density response that relates the charge response $\delta\rho$ to the variation of the external potential, $\delta\rho=\chi\delta v_{\mathrm{ext}}$. The inverse dielectric matrix is then $\varepsilon^{-1}_{\mathbf{GG}'}(\mathbf{q},\omega)=1+v_{\mathbf{G}}(\mathbf{q})\chi_{\mathbf{GG}'}(\mathbf{q},\omega)$. From ε, we derived the macroscopic dielectric function (step 5 in Table I). $\varepsilon_M(\omega)=1/\varepsilon^{-1}_{\mathbf{G}=\mathbf{G}'=0}(\mathbf{q}\to 0,\omega)$,[46,47] and hence absorption and loss spectra for vanishing momentum transfer as $\mathrm{Im}\,\varepsilon_{\mathrm{M}}(\omega)$ and $\mathrm{Im}[1/\varepsilon_M(\omega)]$, respectively.

For the xc kernel we used in particular the model $f_{\mathrm{xc}}^{\mathrm{dyn}}$ of Eq. (3), where α and β were taken at the beginning as independent parameters to be determined by fitting to the experimental absorption spectra (with the exception of CdSe, where α and β were fitted to the BSE result, as the absolute and relative height of the experimental peaks are uncertain). The parameters α and β which gave the best results for the fitting are those listed in Table II. In the following we will use these fitted values to confirm that the parameters can be related by means of Eq. (3) to material dependent physical quantities.

In Ref. 35, calculations for bulk silicon and diamond using the BSE gave frequency dependent xc kernels defined as

$$f_{\mathrm{xc}}^{\mathrm{BSE}}(\mathbf{q},\omega)=\frac{4\pi}{q^2}\{[\varepsilon_M^{\mathrm{BSE}}(\omega)-1]^{-1}-[\varepsilon_M^{\mathrm{RPA}}(\omega)-1]^{-1}\}, \quad (18)$$

where $\varepsilon_M^{\mathrm{BSE}}$ is obtained by solving the BSE and $\varepsilon_M^{\mathrm{RPA}}$ is the RPA dielectric function where GW quasiparticle energies are used. In view of the common point of departure, i.e., the BSE, a comparison with those results is particularly significant. Figure 1 shows, at the example of silicon, that our model f_{xc} is effectively a good approximation for $f_{\mathrm{xc}}^{\mathrm{BSE}}$ calculated in Ref. 35.

B. Optical and loss spectra

For the real and the imaginary part of the dielectric function of Si, GaAs, AlAs, and SiC, an excellent fit to experiments was already obtained[30] using $f_{\mathrm{xc}}^{\mathrm{static}}$. Both static and dynamical LRC calculations produce a nonuniform shift in peak positions and a redistribution of intensities between the peaks. When spectra are calculated with $f_{\mathrm{xc}}^{\mathrm{dyn}}$, using the fitted parameters α and β in Table II, the curves obtained are almost identical to the ones shown in Ref. 30 (for this reason, they are not displayed here). The values of α^{static} used in Ref. 30 (0.22, 0.2, 0.35, and 0.5 for Si, GaAs, AlAs, and SiC, respectively) are evidently larger than the values of α listed in Table II, as they also contain an averaged contribution of the dynamical term dependent on β. Instead, the present values of α are close to the values of α^{static} suitable for the simulation of the static dielectric constant.[30]

It is more interesting to test $f_{\mathrm{xc}}^{\mathrm{dyn}}$ for large-gap materials, like diamond and CdSe. In fact, these materials cannot be described in a satisfactory way[30] using $f_{\mathrm{xc}}^{\mathrm{static}}$. Figures 2 and 3 show the results for the absorption spectra of diamond and CdSe. A broadening of 0.4 eV was used in both cases. The static LRC model (dashed line) already gives a significant improvement (in particular for the absorption threshold and the first shoulder of diamond and for the overall shape of the

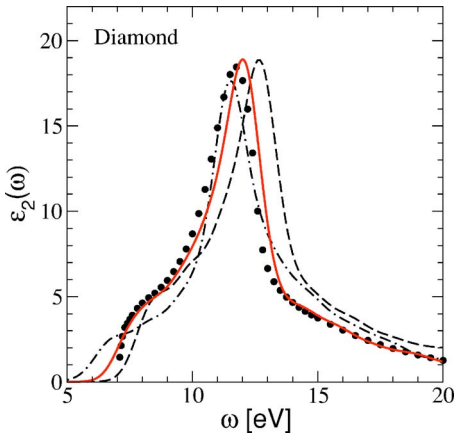

FIG. 2. (Color online) Imaginary part of the macroscopic dielectric function for diamond. Dots experiment; dotted-dashed curve, TDLDA calculation; dashed curve, TDDFT–static LRC calculation; solid line, TDDFT calculation using the dynamical model kernel.

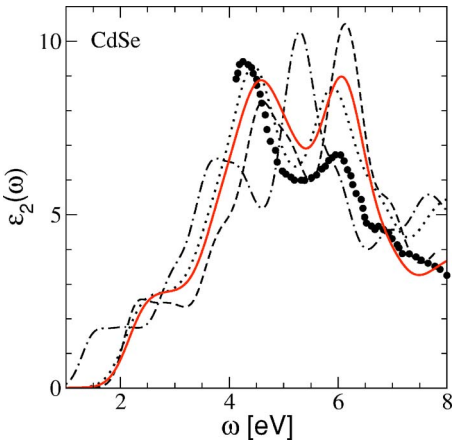

FIG. 3. (Color online) Imaginary part of the macroscopic dielectric function for CdSe. Dots, experiment; dotted-dashed curve, TDLDA calculation; dashed curve, TDDFT–static LRC calculation; solid line, TDDFT calculation using the dynamical model kernel.

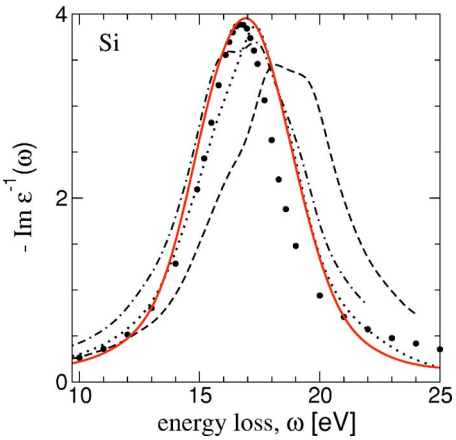

FIG. 4. (Color online) Energy loss function for Si. Dots, experiment; dotted curve, BSE calculation; dashed curve, TDDFT–static LRC ($\alpha^{\mathrm{static}}=0.2$) calculation; dotted-dashed line, TDDFT–static LRC ($\alpha^{\mathrm{static}}=2.0$) calculation; solid line, TDDFT calculation using the dynamical model kernel.

spectrum of CdSe) with respect to the TDLDA calculation (dashed-dotted line), although this approximation does not work nearly as well as for the materials discussed in the preceding paragraph. We can observe in Fig. 2 that a static LRC approximation with $\alpha^{\mathrm{static}}=0.6$ (dashed line) for diamond enhances the shoulder on the low-energy side of the absorption spectrum, but does not give a correct position of the E_2 peak (at about 12 eV). The dynamical model kernel (solid line) corrects completely the E_2 peak position, without increasing too much the oscillator strength of the E_1 peak (at about 8 eV), as it would happen by simply increasing the value of the parameter α^{static} of $f_{\mathrm{xc}}^{\mathrm{static}}$. In the case of CdSe (Fig. 3), the improvement due to the use of the dynamical model is even more striking. It must be pointed out that the experimental results (dots) for the zinc-blende phase of CdSe (Ref. 48) have some uncertainties in both the absolute and the relative heights of the peaks, the authors of Ref. 48 state that only the peak positions are certain. For this reason, we decided to compare our LRC results with the BSE calculation (dotted line). The static LRC calculation (dashed line) is still far away form the BSE curve. As predicted by Eq. (4) of Ref. 30, using the proportionality to the inverse of the experimental dielectric constant, $\alpha^{\mathrm{static}}=0.55$ gives the best overall result. The use of $f_{\mathrm{xc}}^{\mathrm{dyn}}$ (solid line) leads to a sizeable step forward and to a much better agreement with the BSE curve. An analogous agreement with experiment is verified for the real parts of the dielectric functions, both for diamond and CdSe (not shown).

Going up further in frequency, and looking at the EELS, the importance of the frequency dependence of $f_{\mathrm{xc}}^{\mathrm{dyn}}$ becomes even more evident. In fact, the simple LRC method is never working at the same time for absorption and for loss spectra.[30] In Fig. 4 the dashed curve is the static LRC result ($\alpha^{\mathrm{static}}=0.2$, i.e., the value which gives the best absorption spectrum) for the EELS of silicon from Ref. 30. This calculation is in bad agreement with experiment (dots). An excellent agreement with experiment is found when the BSE approach is used (dotted curve, taken from Ref. 49); the full BSE calculation of a valence plasmon is however today still at the limit of computer resources, and one should remember that in this particular case a TDLDA calculation gives comparable results.[49] Actually, one might hope to obtain a real breakthrough using TDDFT for those cases where TDLDA fails. In contrast to the static LRC, the dynamical LRC approach is still valid. The continuous curve is the dynamical LRC result using the same α and β as for the absorption spectrum (see Table II). It is interesting to observe that a comparable result can be obtained using $f_{\mathrm{xc}}^{\mathrm{static}}$, provided that $\alpha^{\mathrm{static}}=2$ (dotted-dashed curve). It can be remarked that $\alpha=2$ is the average value of $f_{\mathrm{xc}}^{\mathrm{dyn}}$ in the frequency range of the plasmon, as it is visible in the inset of Fig. 1.

Finally, one might wonder if this simple model for $f_{\mathrm{xc}}^{\mathrm{dyn}}$ can to some extent account for bound excitons. We consider as an example a LiF crystal, whose experimental absorption spectrum (dots) is shown in Fig. 5. Using the experimental dielectric constant of LiF and Eq. (4) of Ref. 30 we obtain for the constant α^{static} of the static LRC model the value 2.0. This choice of α^{static} gives a reasonable compromise, enhancing slightly the low energy structures without provoking the collapse of the spectrum (see Fig. 5). The worst disagreement concerns the absence of the large excitonic peak at about 12.5 eV. The dynamical model (solid line) with the parameters α and β of Table II improves remarkably the peak positions, and allows to account for the bound exciton peak. Alternatively, a similar agreement can only be found using the BSE approach (dotted line) with a much larger computational effort.[9–11,50]

We comment now on the physical meaning of the parameters α and β of Eq. (3) listed in Table II. The parameter α of $f_{\mathrm{xc}}^{\mathrm{dyn}}$ is proportional to $\omega_g/\omega_p^2\varepsilon(0)$. Moreover, according to Eq. (14), the ratio α/β, gives the square of the resonance frequency ω_g. The resonance frequencies ω_g calculated from the ratio α/β, using the parameters obtained by the fit, are listed in the last column of Table II. We can observe that for all materials except LiF the resonance frequency is consistently in the middle of the region of strong absorption. Using the calculated values of ω_g we can now check if α satisfies the relation of Eq. (14). In Fig. 6 we plot the parameter α as

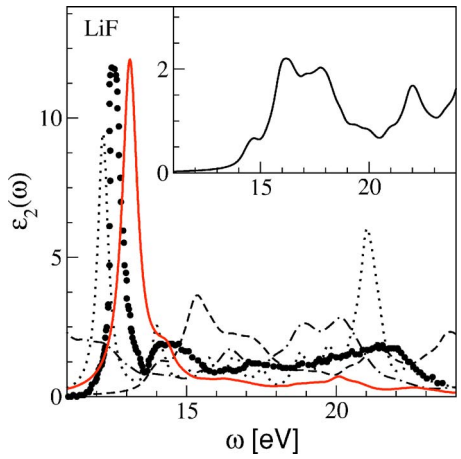

FIG. 5. (Color online) Imaginary part of the macroscopic dielectric function for LiF. Dots, experiment; dotted line, BSE calculation; dotted-dashed curve, TDLDA calculation; dashed curve, TDDFT–static LRC calculation; solid line, TDDFT calculation using the dynamical model kernel. In the inset, RPA calculation using quasiparticle energies.

a function of $\omega_g/\varepsilon_M(0)\omega_p^2$. Except for LiF, all the points are close to a straight line which can be fitted by

$$\alpha = 104.5\frac{\omega_g}{\varepsilon_M(0)\omega_p^2}. \tag{19}$$

For the parameter β we remind that the following holds:

$$\beta = \alpha/\omega_g^2. \tag{20}$$

These results validate our simple model for application to semiconductors and insulators whose absorption spectrum is characterized by strong continuum exciton effects. Considering the results for the EELS of silicon, its validity can be extended to frequencies in the range of the valence plasmon. Now that we know that the model is valid, approximate values for α and β can be obtained through Eqs. (19) and (20)

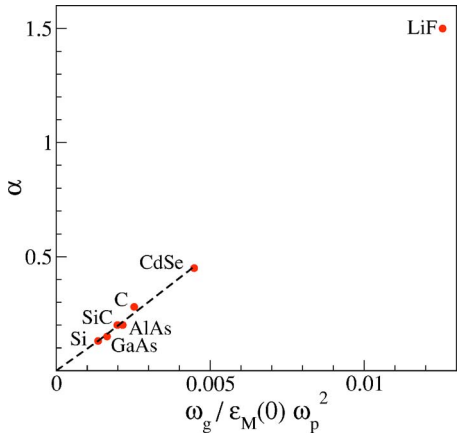

FIG. 6. (Color online) Material dependence of the parameter α. The values displayed are calculated from Table II, except for the case of LiF, where we preferred to use the more realistic average gap $\omega_g=16$ eV (see the inset of Fig. 4).

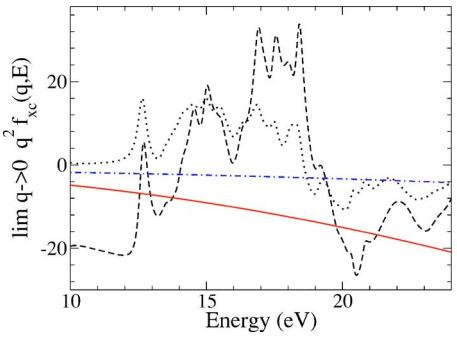

FIG. 7. (Color online) Real (dashed line) and imaginary (dotted line) part of the LRC component of f_{xc}^{BSE} for LiF from Eq. (18). Solid line, f_{xc}^{dyn} using the parameters α and β from the fit; dotted-dashed line, f_{xc}^{dyn} using the parameters predicted by Eqs. (19) and (20) with $\omega_g=16$ eV.

without the need of the fitting procedure, simply starting from the knowledge of the dielectric constant, the plasma frequency and the range of absorption. It is important to notice that Eqs. (19) and (20) are valid not only for the "classical" semiconductors (Si, GaAs, AlAs), which have quite similar plasma frequencies and absorption energy ranges, but also in the case of SiC, diamond and CdSe, where the ratios between plasma and resonance frequencies are very different. Concerning LiF, it turns out that the fitted value of α would be on the straight line (19) if we had used a ω_g of 18 eV (in the middle of the absorption region, see Fig. 4), instead of the value 6.7 eV which comes from the ratio α/β. It is not surprising that the single oscillator approximation at the basis of the derivation of the model (see Sec. II) breaks down in the case of LiF. In fact, the absorption peak of LiF calculated within the RPA and using the quasiparticle energies is very broad (see the inset of Fig. 4), as a consequence also the width of the resonant peak of the oscillator model is as large as 10 eV. Any attempt to generalize the model in order to include the contribution of more oscillators leads to a dependence on ω of the xc kernel more complicated than the simple $\alpha+\beta\omega^2$ form. Moreover, we cannot assure anymore that the contribution of the imaginary part of f_{xc} in Eq. (13) is not important.

In order to shed light onto this problem, we performed a direct calculation of the frequency dependence of f_{xc}^{BSE} for LiF from Eq. (18). The result is displayed in Fig. 7. It turns out that the LRC component of the real part of f_{xc}^{BSE} shows a complicated dependence on ω, characterized by large oscillations. The real part of $f_{xc}^{\mathbf{00}}$ was also calculated by Marini *et al.*,[29] in contrast to our result, their curve is much smoother in the energy range up to 18 eV. This is probably due to the fact that Marini *et al.* take into account the $\mathbf{G},\mathbf{G}'\neq 0$ components of $f_{xc}^{\mathbf{G},\mathbf{G}'}$, which are neglected in our model. In fact, it is known from the work of Sottile *et al.*[26] that an increase of the dimension of the $f_{xc}^{\mathbf{G},\mathbf{G}'}$ matrix leads to a smoothing of the head of $f_{xc}^{\mathbf{00}}$ at low energies, with a consequent shift of the oscillations to higher energies. If we analyze the frequency dependence of our model f_{xc}^{dyn} in Fig. 7 we can see that f_{xc}^{dyn} calculated starting from the fitted parameters gives a better average of f_{xc}^{BSE} in the region of the main peak. On the other hand, f_{xc}^{dyn} calculated with the parameters extracted

from Eqs. (19) and (20) with $\omega_g = 16$ eV describes better an average of $f_{\mathrm{xc}}^{\mathrm{BSE}}$ over the whole absorption region up to 24 eV. This explains why the fitted $f_{\mathrm{xc}}^{\mathrm{dyn}}$ provides an improved excitonic peak, whereas it causes a degraded quality of the absorption spectrum in the energy range 16–24 eV (see Fig. 4, solid line). Finally, we can observe in Fig. 7 that, although the imaginary part of $f_{\mathrm{xc}}^{\mathrm{BSE}}$ is still negligible in the region of the main peak, it is of the same order of magnitude as the real part in most of the absorption frequency range. This may be a factor contributing to the worsening of the agreement between the spectrum calculated with the fitted $f_{\mathrm{xc}}^{\mathrm{dyn}}$ and experiment for energies above the excitonic peak. Besides this limitation, the absorption spectrum yielded by the fitted $f_{\mathrm{xc}}^{\mathrm{dyn}}$ remains extremely satisfactory, showing that this simple dynamical model, in contrast to its static counterpart, can account for bound excitons.

We should observe that the model we are proposing here has proved to be valid for a large variety of semiconductors and insulators, but this fact does not guarantee that the model is in general valid for any semiconductor or insulator. Each time the model is used to calculate the optical or loss spectra of a material, the validity of the underlying approximations must be carefully checked. In general, the model should not be used for a detailed quantitative analysis of the spectra. Although we can always expect an important correction to the peaks which are sensitive to excitonic effects, the quality of the final spectra is dependent on the specific material. Finally, further developments of the present model are still possible. In particular, we already verified that allowing a spatial dependence of the kernel improves considerably the optical spectra of LiF.

IV. CONCLUSIONS

In conclusion, we proposed a model for the xc kernel f_{xc} of TDDFT that contains a static term and a term that depends quadratically on the frequency. Both terms are long ranged. We gave simple expressions for the two parameters of the model that show their connections to important material dependent parameters, i.e., to the dielectric constant, the plasma frequency and the average absorption gap. We showed numerical results for the dielectric function of various semiconductors exhibiting a strong continuum exciton effect, and for bound excitons. Also the electron energy loss spectrum of silicon was discussed. We proved that absorption spectra are systematically improved with respect to results obtained with a static kernel, and that now the whole frequency range, including the region of plasmons, can be covered by the same model. We believe that this approach is a promising alternative to the use of the significantly more complicated kernels proposed in literature for the efficient calculation of electronic excitations in complex systems made of semiconductors and insulators.

ACKNOWLEDGMENTS

This work was partially supported by the EU 6th Framework Programme through the NANOQUANTA Network of Excellence (NMP4-CT-2004-500198). Computer time was granted by IDRIS (project 020544) on the NEC SX5. Ground state and GW calculations were done using ABINIT.[43] TDDFT and BSE calculations were done using, respectively, the DP and EXC codes.[45] The authors are grateful to Miguel Marques and to Andrea Cucca for their help.

[1] P. Hohenberg and W. Kohn, Phys. Rev. **136**, B864 (1964).
[2] W. Kohn and L. J. Sham, Phys. Rev. **140**, A1133 (1965).
[3] L. Hedin, Phys. Scr. **21**, 477 (1980).
[4] R. Del Sole and R. Girlanda, Phys. Rev. B **48**, 11789 (1993).
[5] L. J. Sham and T. M. Rice, Phys. Rev. **144**, 708 (1966).
[6] W. Hanke, Adv. Phys. **27**, 287 (1978).
[7] G. Onida, L. Reining, and A. Rubio, Rev. Mod. Phys. **74**, 601 (2002), and references therein.
[8] G. Onida, L. Reining, R. W. Godby, R. Del Sole, and W. Andreoni, Phys. Rev. Lett. **75**, 818 (1995).
[9] S. Albrecht, L. Reining, R. Del Sole, and G. Onida, Phys. Rev. Lett. **80**, 4510 (1998).
[10] L. X. Benedict, E. L. Shirley, and R. B. Bohn, Phys. Rev. B **57**, R9385 (1998).
[11] M. Rohlfing and S. G. Louie, Phys. Rev. Lett. **81**, 2312 (1998).
[12] E. Runge and E. K. U. Gross, Phys. Rev. Lett. **52**, 997 (1984).
[13] M. A. L. Marques and E. K. U. Gross, Annu. Rev. Phys. Chem. **55**, 427 (2004).
[14] A. Zangwill and P. Soven, Phys. Rev. A **21**, 1561 (1980).
[15] S. Waidmann, M. Knupfer, B. Arnold, J. Fink, A. Fleszar, and W. Hanke, Phys. Rev. B **61**, 10149 (2000).
[16] V. I. Gavrilenko and F. Bechstedt, Phys. Rev. B **55**, 4343 (1997).
[17] P. Ghosez, X. Gonze, and R. W. Godby, Phys. Rev. B **56**, 12811 (1997).
[18] I. V. Tokatly and O. Pankratov, Phys. Rev. Lett. **86**, 2078 (2001).
[19] P. de Boeij, F. Kootstra, J. Berger, R. van Leeuwen, and G. Snijders, J. Chem. Phys. **115**, 1995 (2001).
[20] I. V. Tokatly, R. Stubner, and O. Pankratov, Phys. Rev. B **65**, 113107 (2002).
[21] A. Görling, Phys. Rev. A **57**, 3433 (1998).
[22] Y. H. Kim and A. Görling, Phys. Rev. B **66**, 035114 (2002).
[23] Y. H. Kim and A. Görling, Phys. Rev. Lett. **89**, 096402 (2002).
[24] K. Tatarczyk, A. Schindlmayr, and M. Scheffler, Phys. Rev. B **63**, 235106 (2001).
[25] L. Reining, V. Olevano, A. Rubio, and G. Onida, Phys. Rev. Lett. **88**, 066404 (2002).
[26] F. Sottile, V. Olevano, and L. Reining, Phys. Rev. Lett. **91**, 056402 (2003).
[27] R. Del Sole, G. Adragna, V. Olevano, and L. Reining, Phys. Rev. B **67**, 045207 (2003).
[28] G. Adragna, R. Del Sole, and A. Marini, Phys. Rev. B **68**, 165108 (2003).
[29] A. Marini, R. Del Sole, and A. Rubio, Phys. Rev. Lett. **91**, 256402 (2003).
[30] S. Botti, F. Sottile, N. Vast, V. Olevano, L. Reining, H.-C. Weissker, A. Rubio, G. Onida, R. Del Sole, and R. W. Godby, Phys. Rev. B **69**, 155112 (2004).
[31] F. Bruneval, F. Sottile, V. Olevano, R. Del Sole, and L. Reining,

Phys. Rev. Lett. **94**, 186402 (2005).
[32] R. Stubner, I. V. Tokatly, and O. Pankratov, Phys. Rev. B **70**, 245119 (2004).
[33] F. Sottile, K. Karlsson, L. Reining, and F. Aryasetiawan, Phys. Rev. B **68**, 205112 (2003).
[34] S. Botti, N. Vast, L. Reining, V. Olevano, and L. C. Andreani, Phys. Rev. B **70**, 045301 (2004).
[35] R. Del Sole, G. Adragna, V. Olevano, and L. Reining, Phys. Rev. B **67**, 045207 (2003).
[36] We verified that using only the element $\mathbf{G}=\mathbf{G}'=0$ of the kernel of Eq. (4) gives very good absorption spectra for all the materials considered in this study, even for the most problematic case of LiF.
[37] C. Kittel, *Introduction to Solid State Physics*, 7th ed. (Wiley, New York, 1996).
[38] M. Altarelli, D. L. Dexter, H. M. Nussenzveig, and D. Y. Smith, Phys. Rev. B **6**, 4502 (1972).
[39] J. Rowe and D. Aspnes, Phys. Rev. Lett. **25**, 162 (1970).
[40] J. Rowe and D. Aspnes, Phys. Rev. Lett. **25**, 979(E)(1970).
[41] R. M. Martin, J. A. van Vechten, J. E. Rowe, and D. E. Aspnes, Phys. Rev. B **6**, 2500 (1972).
[42] We give here some details of calculations for CdSe and LiF, as these materials were not considered in Ref. 30. We used norm-conserving Trouiller and Martins pseudopotentials and a plane-wave basis with a kinetic energy cutoff of 30 Ry for CdSe and 80 Ry for LiF. The GW eigenvalues were calculated using the method of Ref. 44. The spectra for CdSe were obtained using 864 off-symmetry shifted k points in the Brillouin zone, whereas only 256 off-symmetry shifted k points were needed for LiF.
[43] X. Gonze *et al.*, Comput. Mater. Sci. **25**, 478 (2002); http://www.abinit.org
[44] R. W. Godby and R. J. Needs, Phys. Rev. Lett. **62**, 1169 (1989).
[45] http://theory.lsi.polytechnique.fr/codes/
[46] S. L. Adler, Phys. Rev. **126**, 413 (1962).
[47] N. Wiser, Phys. Rev. **129**, 62 (1963).
[48] C. Janowitz, O. Günther, G. Jungk, R. L. Johnson, P. V. Santos, M. Cardona, W. Faschinger, and H. Sitter, Phys. Rev. B **50**, 2181 (1994).
[49] V. Olevano and L. Reining, Phys. Rev. Lett. **86**, 5962 (2001).
[50] M. Rohlfing and S. G. Louie, Phys. Rev. B **62**, 4927 (2000), and references therein.